South African Journal of Chemical Engineering 55 (2026) 551–559

Contents lists available at ScienceDirect

South African Journal of Chemical Engineering

journal homepage: www.elsevier.com/locate/sajce

Spherical and rod-shaped nanocellulose from filter paper waste: A comparative study of acid hydrolysis

Zahrotul Istiqomah [a,*], Holilah [b,*], Didik Prasetyoko [a], Sri Sunarmi [a], Hendro Juwono [a], Agus Wedi Pratama [c], Mohd Saiful Asmal Rani [d], Dina Wahyu Indriani [e], Victor Feizal Knight [f], Mohd Nor Faiz Norrrahim [f,*]

[a] Department of Chemistry, Faculty of Science and Data Analytics, Institut Teknologi Sepuluh Nopember Keputih, Sukolilo Surabaya 60111, Indonesia
[b] Research Center for Biomass and Bioproducts, National Research and Innovation Agency of Indonesia (BRIN), Serpong, South Tangerang 15314, Banten, Indonesia
[c] Department of Agrotechnology, Faculty of Agriculture, University of Jember, Jember, Indonesia
[d] Department of Physics, Faculty of Science, Universiti Putra Malaysia, 43400 UPM Serdang, Selangor, Malaysia
[e] Department of Biosystem Engineering, Faculty of Agricultural Technology, Universitas Brawijaya, Jalan Veteran Malang, Indonesia
[f] Research Center for Chemical Defence, Defence Research Institute, Universiti Pertahanan Nasional Malaysia, Kem Sungai Besi, 57000 Kuala Lumpur, Malaysia

ARTICLE INFO

Keywords:
Filter paper waste
Nanocrystalline cellulose
Acid hydrolysis
Organic acid

ABSTRACT

Filter paper waste represents a significant yet underutilized feedstock for producing nanocellulose, a high-value nanomaterial essential for bioplastics and nanocomposites due to its biodegradability and mechanical strength. Valorizing this laboratory byproduct supports circular economy principles by converting waste into functional materials. In this study, nanocellulose was successfully isolated from filter paper waste (FPW). Cellulose extracted from the FPW was converted into nanocrystalline cellulose (NCC) through acid hydrolysis using two inorganic acids (sulfuric and hydrochloric) and two organic acids (citric and formic). The results revealed that acid type significantly influences particle morphology: hydrolysis with inorganic acids yielded spherical NCC particles, while the organic acids produced thin rod-shaped NCC. The average particle diameters of NCC from sulfuric and hydrochloric acid were 42.08 nm and 53.14 nm, respectively. FPW-NCH exhibited the highest crystallinity (87.40%), while FPW-NCS showed the lowest thermal stability (degradation onset at 220 °C). These findings demonstrate that simple acid selection is a critical tool for tailoring nanocellulose properties for specific end-use requirements

1. Introduction

The increasing global demand for sustainable materials has spurred significant interest in nanocellulose, a bio-derived nanomaterial with remarkable properties (Y. Chen et al., 2021; Nitodas et al., 2023). Nanocellulose, encompassing both nanocrystalline cellulose (NCC) and cellulose nanofibrils, exhibits high mechanical strength, excellent thermal stability, optical transparency, and biodegradability, making it a promising candidate for diverse applications, ranging from nanocomposites and bioplastics to biomedical, wound healing, and protective filtration materials (S. Chen et al., 2021; Ee et al., 2022; Firmanda et al., 2024; Khalili et al., 2025; Mahardika et al., 2025; Meneguin, 2021; Vinanthi Rajalakshmi et al., 2025). These desirable characteristics stem from the unique hierarchical structure of cellulose, composed of highly ordered crystalline regions interspersed with amorphous domains. While traditionally sourced from wood pulp, the exploration of alternative, more sustainable, and readily available cellulose sources is crucial for large-scale production and cost-effectiveness. This pursuit has led researchers to investigate various agricultural residues and industrial byproducts as potential feedstocks (Collazo-Bigliardi et al., 2018; Padhi et al., 2023; Pratama et al., 2024b; Syafri et al., 2022).

One such underutilized resource is filter paper waste. While commonly generated in laboratory operations for chemical analysis and separation, filter papers are also ubiquitous in industrial filtration systems, automotive air/oil filtration, and healthcare facilities (Hassan et al., 2020). Currently, this high-purity cellulosic material is often discarded, contributing to waste accumulation. However, filter paper, primarily composed of high-quality cellulose, presents a valuable and readily available feedstock for nanocellulose production (Hassan et al., 2020). Repurposing this waste stream aligns with the principles of a

* Corresponding authors.
E-mail addresses: istiqomahzahrotul@gmail.com (Z. Istiqomah), holi003@brin.go.id (Holilah), faiz@upnm.edu.my (M.N.F. Norrrahim).

https://doi.org/10.1016/j.sajce.2025.12.017
Received 16 October 2025; Received in revised form 22 December 2025; Accepted 27 December 2025
Available online 28 December 2025

circular economy, offering a sustainable solution for waste management and resource utilization (Velenturf and Purnell, 2021). Furthermore, utilizing waste filter paper could potentially reduce the environmental impact associated with traditional cellulose sourcing.

The production of NCC typically involves acid hydrolysis, a process that selectively removes the amorphous regions of cellulose, leaving behind highly crystalline nanoparticles. Both inorganic acids, such as sulfuric and hydrochloric acid, and organic acids, like citric and formic acid, have been employed for this purpose. The choice of acid and the hydrolysis conditions significantly influence the properties of the resulting NCC, including its size, crystallinity, and surface functionality (Holilah et al., 2022; Wahyudi et al., 2025). Holilah et al. (2022) synthesized nanocellulose using organic acids like formic, lactic, and oxalic acid. Ioelovich (2012) employed sulfuric acid (H_2SO_4) hydrolysis, varying reaction temperature and acid-to-cellulose ratio, achieving nanocellulose with dimensions of $150–200\times10^{-20}$ nm. Brito et al. (2012) utilized 64 % sulfuric acid hydrolysis, producing nanocellulose with a diameter of 5–8 nm and a length of 100–130 nm. Sulfuric acid is the dominant acid used in nanocellulose production because it uniquely enables the creation of highly stable cellulose nanocrystals (NCC) (Holilah et al., 2022). Its primary effect is the selective hydrolysis and removal of the amorphous regions of the cellulose fiber, leaving behind the stiff, crystalline domains (Septevani et al., 2020). Crucially, the sulfate ions from the acid esterify with the hydroxyl groups on the surface of the resulting NCC. This introduces anionic sulfate groups, which give the NCC a strong negative surface charge (high zeta potential). This negative charge is responsible for the powerful electrostatic repulsion that prevents particle aggregation, allowing the NCC to form a stable colloidal suspension in water (Holilah et al., 2024). However, this functionalization is also a drawback, as the sulfate groups catalyze dehydration reactions upon heating, resulting in lower thermal degradation temperature compared to other nanocellulose forms (Johar et al., 2012). The performance of other acids differs mainly in this surface functionalization; hydrochloric acid, while an effective hydrolyzing agent that produces high-crystallinity NCC, does not introduce stabilizing functional groups, leading to poor colloidal stability and particle aggregation (Guo et al., 2020). Conversely, HCl-produced NCC have a higher thermal stability because they lack the catalytic sulfate groups. Phosphoric acid and organic acids offer milder hydrolysis and can introduce different stabilizing groups (like phosphate or carboxyl groups), but they typically result in less uniform particle size and are generally less effective at generating the high colloidal stability that is the hallmark of H_2SO_4-produced NCC (Holilah et al., 2022). While inorganic acids are commonly used, organic acids offer a potential for nanocellulose production (Melenia et al., 2024).

The selection of organic acids (such as citric, maleic, lactic, or formic acid) for nanocellulose production, particularly via acid hydrolysis, is primarily driven by the desire for a sustainable, greener, and safer process, aligning with recent advancements in eco-friendly nanomaterial synthesis (Mosleh-Shirazi et al., 2025). In addition, nanocellulose production by organic acid yields a product with desirable thermal and surface properties when compared to conventional mineral acids like sulfuric or hydrochloric acid (Holilah et al., 2023). The use of strong mineral acids, especially sulfuric acid, is highly effective at cleaving the amorphous regions of cellulose but introduces sulfate groups that reduce the thermal stability of the resulting nanocellulose (a significant drawback for high-temperature applications) and are highly corrosive and difficult to recover, leading to greater environmental concerns and disposal costs (Emam et al., 2020; Ramadhani et al., 2022). In contrast, organic acids offer a milder and less corrosive alternative, often allowing for easier acid recovery and recycling (e.g., via crystallization), aligning with green chemistry principles (Wahyudi et al., 2025). Furthermore, organic acids like citric acid introduce carboxyl (COOH) functional groups onto the nanocellulose surface, which provides a tunable surface chemistry for subsequent modifications and contributes to good colloidal stability in aqueous suspension, while often maintaining or even enhancing the thermal stability of the final nanocellulose product (Nagarajan et al., 2020).

Based on these premises, the central argument of this study is that the chemical nature of the hydrolyzing acid, specifically the difference between strong mineral acids and mild organic acids, serves as the primary determinant in directing the morphological evolution and thermal properties of the resulting nanocellulose. While previous works have treated acid hydrolysis primarily as a top-down depolymerization process, we hypothesize that organic acids can function as shape-preserving agents that maintain the rod-like integrity and high crystallinity of the original cellulose fibers, unlike the aggressive depolymerization often seen with strong mineral acids. To validate this, we conducted a comparative study isolating NCC from filter paper waste using two inorganic acids (H_2SO_4, HCl) and two organic acids (citric, formic). This research aims to resolve the trade-off between colloidal stability and thermal resistance, providing a clear rationale for acid selection based on the targeted end-use application.

2. Experimental

This study was designed based on the hypothesis that the use of mild organic acids in hydrolysis would preserve the rod-like morphology of cellulose crystals better than strong mineral acids. To verify this, the experimental procedure was divided into three main stages: (1) pretreatment of filter paper waste to isolate pure cellulose, (2) comparative acid hydrolysis using four different acids to generate nanocellulose, and (3) comprehensive characterization of the resulting nanoparticles.

2.1. Materials

The filter paper waste used in this study was obtained from the Fundamental Chemistry Laboratory, Department of Chemistry, Institut Teknologi Sepuluh Nopember, Indonesia. Sodium hydroxide (NaOH, ≥99 %), sulfuric acid (H_2SO_4, 98 %), hydrochloric acid (HCl, 37 %), hydrogen peroxide (H_2O_2, 30 % (w/w) in H_2O), citric acid monohydrate ($C_6H_8O_7$, ≥99.5 %), and formic acid (HCOOH, 95 %) were purchased from Sigma Aldrich, Singapore.

2.2. Preparation of filter paper waste

The FPW was soaked in distilled water, milled into pulp, and dried. To ensure the complete removal of any residual lignin, hemicellulose, and contaminants from the waste, the FPW powder was treated with a 10 % hydrogen peroxide and 5 % NaOH solution. The mixture was stirred for 1 h at 100 °C to facilitate effective bleaching and alkalization.

2.3. Hydrolysis of FPW-C using various acids

To selectively depolymerize the amorphous regions of cellulose while retaining the crystalline domains, the hydrolysis process was carried out by mixing FPW with 100 mL of 6 M sulfuric acid (ratio 1:50). These specific reaction conditions (6 M acid concentration, 90 °C, 3 h) were selected to optimize the trade-off between hydrolysis rate and thermal degradation. While higher acid concentrations (e.g., >60 % H_2SO_4) are commonly used at lower temperatures, they pose a higher risk of charring and over-degradation. By using a moderate concentration of 6 M, a higher temperature of 90 °C was required to provide the necessary activation energy to selectively depolymerize the amorphous regions while preserving the crystalline domains, consistent with protocols for controlled acid hydrolysis (Ioelovich, 2012; Guo et al., 2020). The mixture was stirred for 3 h at 90 °C, and centrifuged to separate the solids and filtrate. The obtained solids were added to distilled water and soaked in a cellulose dialysis membrane (MWCO 12,000–14,000 Da) for 5 days. The water was changed every 6 h. The pH was monitored using a digital pH meter until it stabilized at neutral (pH 6–7). After reaching a neutral pH, the mixture was separated by centrifugation. The sample

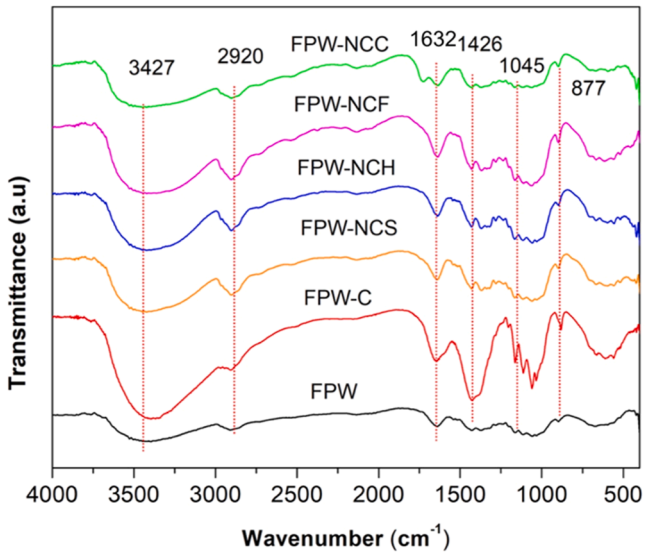

Fig. 1. FTIR spectra of FPW, FPW-C, and nanocellulose of FPW (FPW-NCC and FPW-NCF).

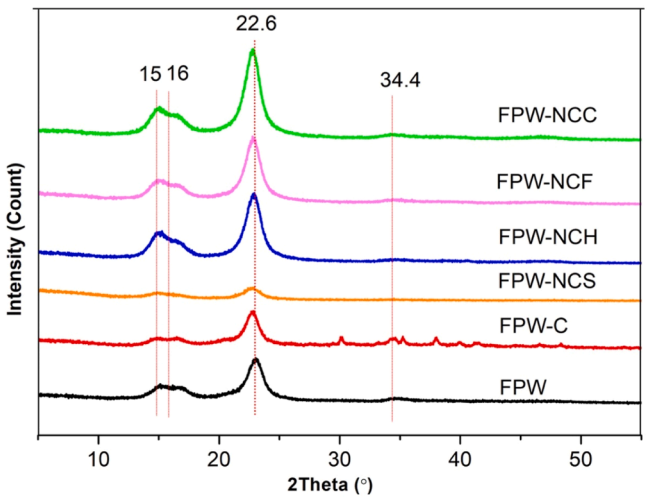

Fig. 2. XRD patterns of FPW, FPW-C, and nanocellulose samples (FPW-NCS, FPW-NCH, FPW-NCF, FPW-NCC).

was repeated using hydrochloric, formic, and citric acids. The results were labelled FPW-NCS (sulfuric), FPW-NCH (hydrochloric), FPW-NCF (formic), and FPW-NCC (citric). To ensure reproducibility, the hydrolysis experiment for each acid type was replicated three times ($n = 3$). The morphological data (particle diameter and length) presented in this study represent the average of at least 100 individual particles measured from TEM images using ImageJ software. Data are expressed as mean ± standard deviation where appropriate.

2.4. Characterization

Fourier transform infrared (FTIR) spectroscopy (Shimadzu Instrument Spectrum One 8400S) was used to analyze the functional groups of the samples. The crystallinity of FPW, cellulose, and NCC was characterized by X-ray diffraction (A Philips-binary Xpert Model diffractometer). The crystallinity index (CrI) was calculated using the Segal method (Segal et al., 1959):

$$CrI(\%) = \frac{I_{200} - I_{am}}{I_{200}} \times 100$$

where $I_{(200)}$ is the maximum intensity of the (200) crystalline peak (around 22°), and $I_{(am)}$ is the minimum intensity at approximately 18°, representing the amorphous region. The calculated CrI values are now presented and discussed to quantitatively demonstrate the effect of hydrolysis and treatment on cellulose crystallinity. Scanning Electron Microscopy (SEM) (Hitachi, FlexSEM 1000) equipped with an Energy Dispersive X-ray Spectroscopy (EDS) detector was used to simultaneously examine the surface morphology and determine the elemental composition of the FPW and nanocellulose samples. The EDS analysis was specifically performed to detect residual inorganic elements derived from the acid hydrolysis treatments. The structure and morphology of the nanocrystalline cellulose component were examined using transmission electron microscopy (TEM, Hitachi HT-7700). Thermogravimetric analysis (TGA/DTG) was performed under a nitrogen atmosphere with a heating ramp of 10° C/min from room temperature to 600°C, to determine the activation temperature of the materials.

3. Results and discussion

The following sections present a systematic analysis of the isolated nanocellulose properties. First, the chemical changes and functional group modifications induced by different acids are confirmed via FTIR. Subsequently, the impact on crystal structure and thermal stability is evaluated. Finally, the morphological evolution from fibers to spherical or rod-shaped nanoparticles is discussed to validate the initial hypothesis regarding acid-directed shape control.

3.1. Analysis of functional groups

FTIR was employed to analyze the functional groups present in nanocrystalline cellulose (NCC) derived from FPW through various acid hydrolysis methods. The FTIR spectra (Fig. 1) illustrate differences in the chemical structure of FPW, its cellulose form (FPW-C), and the NCC produced using different acids: sulfuric acid (FPW-NCS), hydrochloric acid (FPW-NCH), formic acid (FPW-NCF), and citric acid (FPW-NCC). The spectra provide chemical evidence of the successful removal of non-cellulosic impurities and the preservation of the cellulose structure during acid hydrolysis. In the raw FPW spectrum, the broad absorption band centered at 3427 cm^{-1} corresponds to O—H stretching vibrations (Barbosa et al., 2019; Pratama et al., 2024a; Ratna et al., 2023; Sai Prasanna and Mitra, 2020). Upon chemical treatment to produce FPW-C, this band became sharper and more defined, indicating the removal of amorphous hemicellulose and lignin which facilitates stronger intramolecular hydrogen bonding within the remaining cellulose (Pratama et al., 2026).

Crucially, the effectiveness of the bleaching and alkalization process is confirmed by changes in the fingerprint region. The absence of characteristic peaks typically associated with hemicellulose (C=O stretching at ~1730 cm^{-1}) and lignin (aromatic skeletal vibrations at ~1510 cm^{-1}) in the FPW-C and nanocellulose spectra confirms the high purity of the isolated cellulose.

Following acid hydrolysis, the spectral profiles of all nanocellulose samples (FPW-NCS, FPW-NCH, FPW-NCF, and FPW-NCC) remained structurally similar to FPW-C, indicating that the acid treatment depolymerized the cellulose without degrading its core chemical backbone. The persistent peaks at 1045 cm^{-1} (C—O—C pyranose ring skeletal vibration) and 877 cm^{-1} (C—H rocking vibration at the β-glycosidic linkage) confirm that the cellulose I structure was maintained across both inorganic and organic acid treatments. Additionally, the peak at 1632 cm^{-1} (O—H bending of absorbed water) reflects the hydrophilic nature of the nanocellulose surface, which is critical for its dispersion in aqueous media (Pratama et al., 2024b). In addition, the absorption band at 1426 cm^{-1} is associated with the bending vibration of symmetric CH_2 (Holilah et al., 2022).

Table 1
The crystallinity index of FPW, FPW-C, and all FPW-nanocellulose.

Sample	Cystallinity (%)
FPW	73.43
FPW-C	77.72
FPW-NCS	67.37
FPW-NCH	87.40
FPW-NCF	85.23
FPW-NCC	87.44

3.2. Phase and crystallinity analyses

Fig. 2 presents the XRD patterns of filter paper waste (FPW), bleached FPW (FPW-C), and FPW hydrolyzed with various acids. All samples exhibit characteristic cellulose peaks at 2θ: 14.9°, 16.7°, 22.8°, and 34.4° In the FPW sample, the peak at 2θ = 23.1° shifts to 2θ = 22.8° after bleaching, indicating a change in the cellulose structure. The dominant peak in the hydrolyzed samples is observed at 2θ = 22.8° Following acid hydrolysis, two broad peaks emerge at 2θ: 14.9° and 16.7°, along with the peak at 2θ = 22.8° This suggests the formation of cellulose crystals as lignin fragments are removed.

To quantify the changes in crystal structure, the Crystallinity Index (CrI) was calculated using the Segal method. As shown in Table 1, the choice of acid had a profound quantitative impact on the crystal integrity. FPW-NCH exhibited the highest crystallinity of 87.40 %, confirming that HCl hydrolysis effectively removes amorphous regions while preserving the crystalline domains. In stark contrast, the sample hydrolyzed with sulfuric acid (FPW-NCS) showed a significant reduction in crystallinity to 67.37 %. This quantitative drop of approximately 20 % supports the hypothesis that the introduction of sulfate groups by H_2SO_4 causes surface defects and disrupts the hydrogen bonding network within the cellulose lattice, as visibly reflected in the lower intensity of the I_{200} peak.

This disparity is attributed to the distinct reaction mechanisms of the inorganic acids. Sulfuric acid introduces negatively charged sulfate ester groups (OSO_3^-) onto the cellulose surface. While these groups provide colloidal stability, they disrupt the intermolecular hydrogen bonding network and introduce defects into the crystal lattice, thereby lowering crystallinity (Roman and Winter, 2004). In contrast, HCl acts as a non-derivatizing acid; it selectively cleaves the β−1,4-glycosidic bonds in the amorphous regions without grafting functional groups. Consequently, the ordered structure of the crystalline domains remains intact, yielding NCC with a high degree of crystallinity (Holilah et al., 2022).

Similarly, the FPW hydrolyzed with citric acid (FPW-NCC) displays a higher intensity at 2θ = 22.8° compared to the FPW hydrolyzed with formic acid (FPW-NCF), suggesting that citric acid promotes greater crystallinity. This difference arises from the varying molecular structures of the two acids. Formic acid (HCOOH), with its single carboxylic group (COOH), is structurally simpler than citric acid ($C_6H_8O_7$), which possesses three carboxylic groups. The more complex molecular structure of citric acid likely facilitates a more ordered arrangement of atoms within the crystal lattice, resulting in higher crystallinity. While both formic and citric acids can form hydrogen bonds, the intermolecular interactions involving citric acid are more diverse and complex due to its multiple carboxyl groups. These stronger and more complex interactions in citric acid contribute to a more organized atomic arrangement and, consequently, increased crystallinity, as demonstrated in Fig. 2 and Table 1.

3.3. Analysis of thermal stability

Thermal analysis was conducted on FPW to evaluate its thermal stability and determine its decomposition temperature, revealing the temperature at which the material undergoes chemical changes and

Table 2
Thermal analysis data of FPW, FPW-C, and all FPW-nanocellulose.

Samples	Degradation thermal (°C)		W at 600 °C (%)
	Initial (T_o)	Peak (T_p)	
FPW	280	350	18,44
FPW-NCS	220	310	40,96
FPW-NCH	280	365	42,13
FPW-NCF	290	363	35,31
FPW-NCC	280	362	38,61

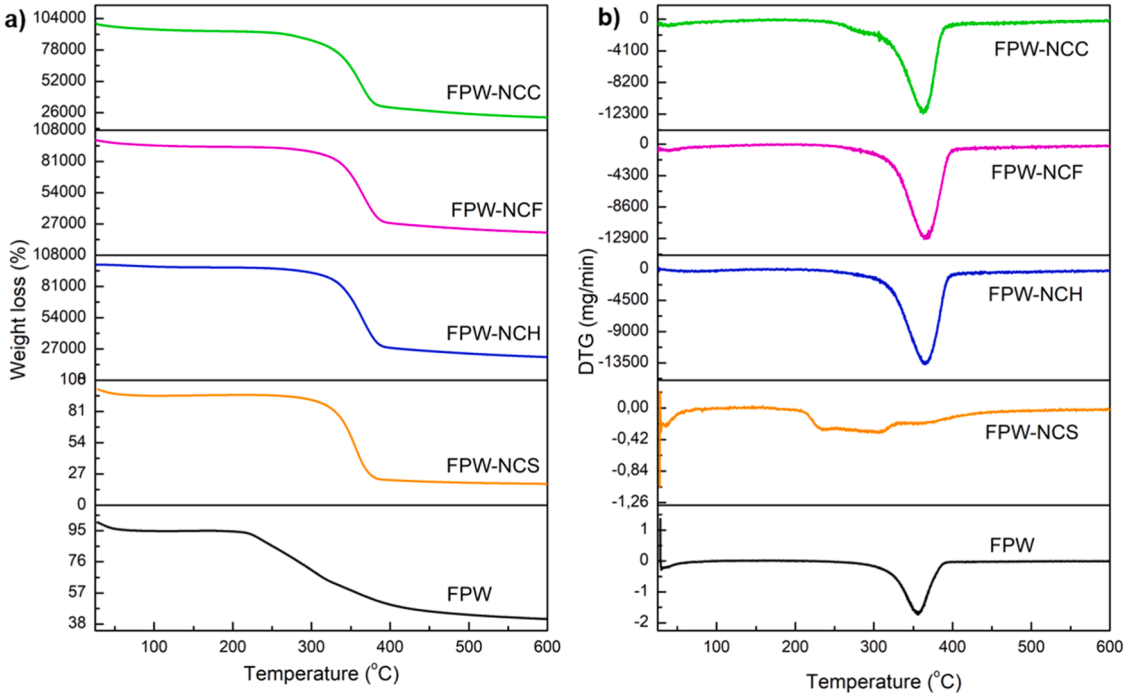

Fig. 3. The TGA (a) and DTG (b) curves of FPW, FPW-C, and all FPW-nanocellulose.

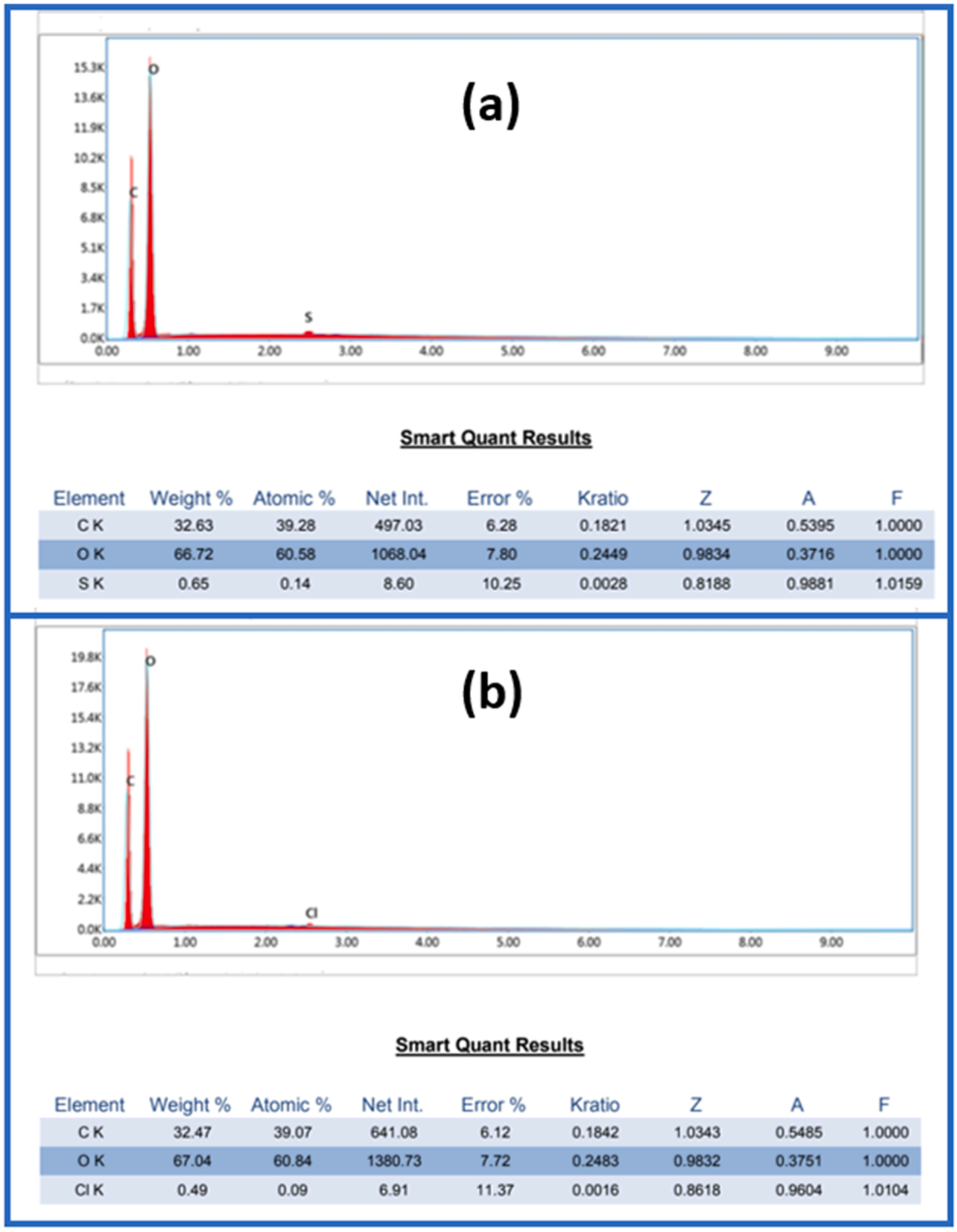

Fig. 4. Energy Dispersive X-ray Spectroscopy (EDS) spectra confirming the presence of residual inorganic ions: (a) Sulfur signal in FPW-NCS, and (b) Chlorine signal in FPW-NCH.

experiences weight loss. Fig. 3 displays the thermogravimetric analysis (TGA) curves for FPW, bleached FPW (FPW-C), and nanocrystalline cellulose derived from FPW-C. The corresponding data have been summarized in Table 2. The initial degradation temperature, indicative of the onset of thermal degradation, was 280 °C for FPW, FPW-NCH, and FPW-NCC, suggesting good thermal stability at this temperature. FPW-NCS exhibited the lowest initial degradation temperature at 220 °C, indicating a faster degradation rate compared to the other samples. Higher initial degradation temperature signifies better heat resistance; in this context, FPW-NCF, with an initial degradation temperature of 290 °C, demonstrated the highest thermal stability among all samples.

The maximum degradation temperature, representing the temperature at which the thermal degradation rate is highest, was observed at 365 °C for FPW-NCH, followed closely by FPW-NCF at 363 °C and FPW-NCC at 362 °C. These higher maximum degradation temperatures suggest that these materials can withstand heat for a longer period before reaching their maximum degradation point. FPW-NCS exhibited the lowest maximum degradation temperature at 310 °C, indicating that it reached its maximum degradation state most rapidly.

At 600 °C, the percentage mass loss provides insight into the amount

Table 3
Comparative summary of particle size, crystallinity index, and thermal degradation of nanocellulose.

Sample	Average Particle Size (nm)	Crystallinity Index (%)	Degradation Initial Temperature (°C)	Degradation Onset Temperature (°C)	Interpretation
FPW-NCS	42.08	67.37	220	310	Sulfated surface; high substitution causes lower CI
FPW-NCH	53.14	87.40	280	365	Higher crystallinity; minimal surface modification
FPW-NCF	36.80	85.23	290	363	Weak acid; well-preserved crystal domains
FPW-NCC	46.23	87.44	280	362	Weak acid, Esterified surface but highly crystalline

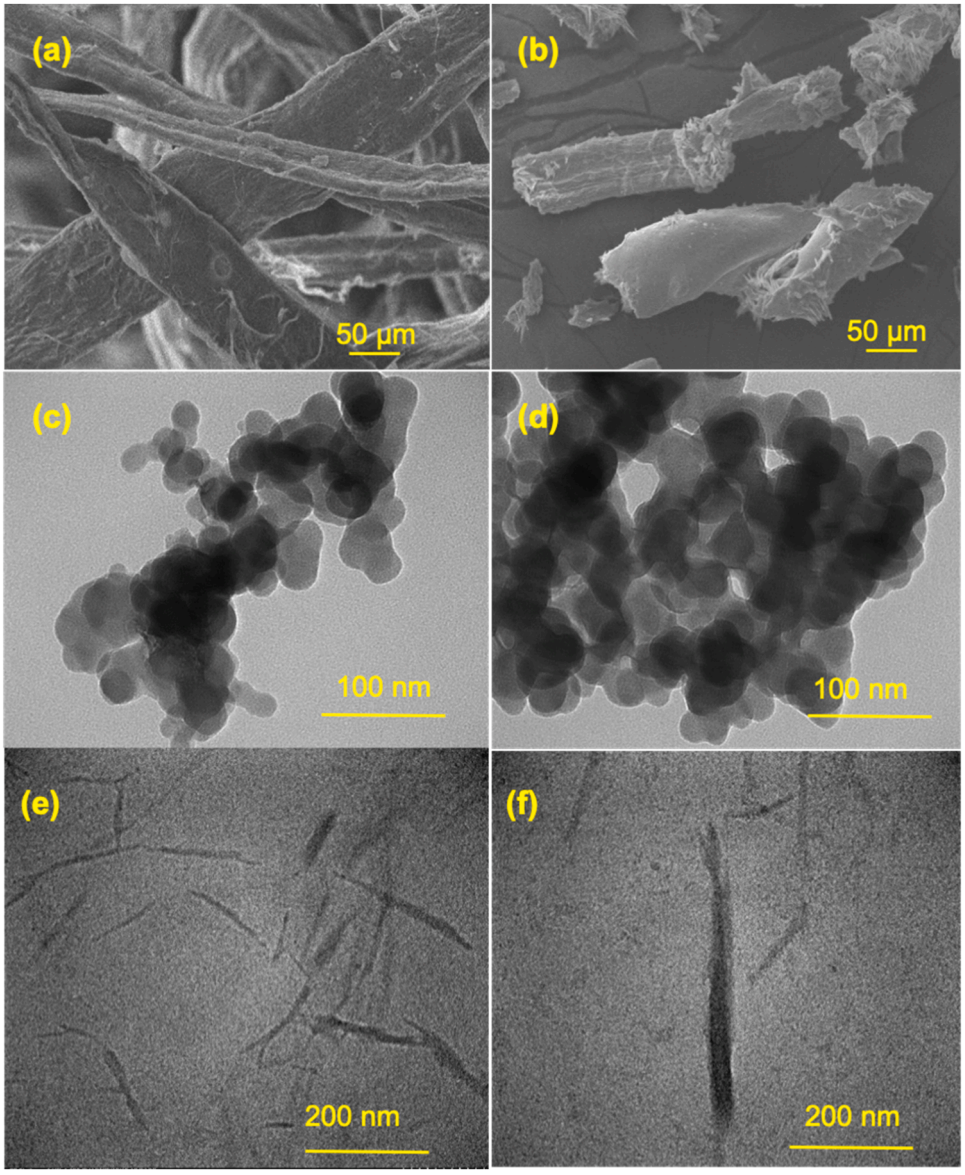

Fig. 5. The SEM image of (a) FPW and (b) FPW-C, and the TEM image of (c) FPW-NCS, (d) FPW-NCH, (e) FPW-NCF, and (f) FPW-NCC.

of material remaining after thermal degradation. FPW exhibited the lowest mass loss (18.44 %), indicating relatively high residual stability. FPW-NCH showed the highest mass loss (42.13 %), closely followed by FPW-NCS (40.96 %). This suggests that FPW possesses a structure more resistant to thermal degradation at high temperatures compared to the chemically modified samples.

The higher inorganic residue observed in some samples, particularly FPW-NCS, can be attributed to the residual sulfate anions from the sulfuric acid used in the hydrolysis process. These sulfate residues can hinder the combustion process, as noted in the previous work (Holilah et al., 2022). The type of acid used in the treatment, whether inorganic or organic, significantly influences the amount of residue remaining after thermal analysis.

To further elucidate the mechanism behind the reduced thermal

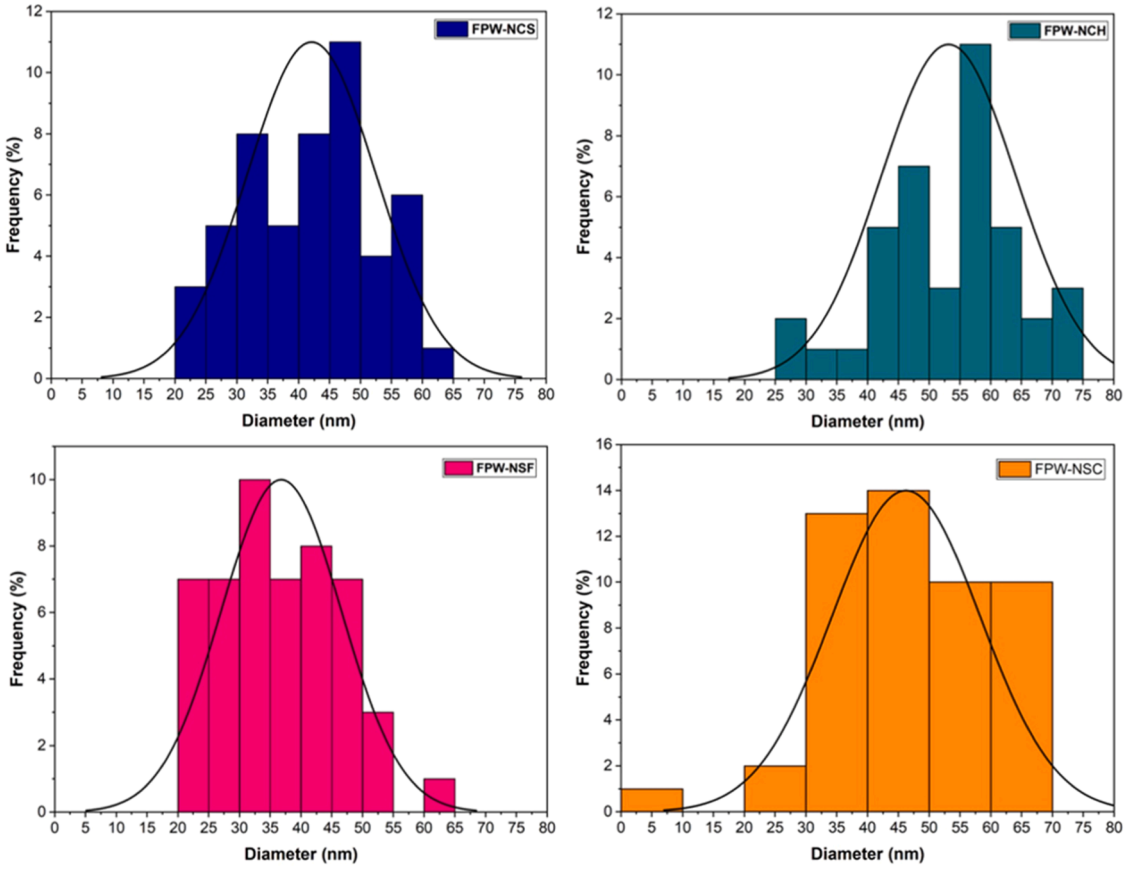

Fig. 6. Diameter distributions of FPW-NCS, FPW-NCH, FPW-NCF, and FPW-NCC.

stability of the mineral acid-hydrolyzed samples, elemental analysis was conducted using EDS. Fig. 4 presents the EDS spectra for FPW-NCS and FPW-NCH. The spectrum for FPW-NCS (Fig. 4a) clearly reveals a characteristic peak for sulfur (S) with a concentration of 0.65 wt %, confirming the presence of sulfate half-ester groups introduced during sulfuric acid hydrolysis. These sulfate groups are known to facilitate the dehydration of cellulose chains, thereby catalyzing thermal degradation at lower temperatures (Roman and Winter, 2004). This explains why FPW-NCS exhibited the lowest Tonset (220 °C).

Similarly, the EDS spectrum for FPW-NCH (Fig. 4b) detects residual chlorine (Cl) at 0.49wt %. While the presence of chlorine indicates acid residue, the degradation effect is most pronounced in the sulfate-containing sample. The absence of such mineral residues in the formic and citric acid-hydrolyzed samples correlates with their superior thermal stability, as observed in the TGA curves.

Comparative summary of particle size, crystallinity index, and thermal degradation of nanocellulose is shown in Table 3. This integrative summary helps visualize how crystallinity and surface modification influence the thermal stability of the nanocellulose.

3.4. Morphological analysis

The morphology of FPW and FPW-C was examined using SEM, with the results shown in Fig. 5(a) and (b). Both FPW and FPW-C exhibit rod-like shapes, but FPW-C displays a cleaner and smoother fiber surface. This improvement is due to the bleaching process, which effectively removes residual dye and impurities from the used filter paper (Klunklin et al., 2023). Transmission electron microscopy (TEM) analysis, coupled with ImageJ software, was employed to investigate the morphology and size distribution of the resulting nanocellulose particles (Fig. 5(c–f)).

Nanocellulose derived from FPW-C through hydrolysis with inorganic acids (sulfuric and hydrochloric acid) presented a network of interconnected spherical particles. This network formation is likely facilitated by the development of interfacial hydrogen bonds between the nanocellulose spheres. Particle size analysis, conducted on over 100 randomly selected particles ($n > 100$) using ImageJ software, revealed that the diameters of these spheres were predominantly below 100 nm (Fig. 6). Specifically, the average particle diameters for nanocellulose hydrolyzed with sulfuric acid and hydrochloric acid were 42.08 ± 4.12 nm and 53.14 ± 3.42 nm, respectively.

In contrast, hydrolysis with organic acids (formic and citric acid) resulted in nanocellulose with a short rod-like fiber morphology. While the morphology differed, the particle size distribution remained similar to that of the inorganically derived nanocellulose, with diameters also below 100 nm. The particle size distributions for nanocellulose hydrolyzed with formic acid and citric acid were 36.80 nm and 46.23 nm, respectively. The observed morphological differences may be attributed to the generally lower hydrolysis ability of organic acids compared to inorganic acids.

The limitation of previous studies has often been the focus on a single type of acid, typically sulfuric acid, which limits the control over particle geometry. Our results advance this understanding by demonstrating a clear dichotomy in morphological evolution driven by acid strength. The formation of spherical nanoparticles by inorganic acids (H_2SO_4, HCl) observed in this study aligns with the 'cutting' mechanism of strong acids, which aggressively attack not only the amorphous regions but also the defects on crystal surfaces, acting like a 'peeling' process that rounds the particle edges (Holilah et al., 2022).

In contrast, the preservation of rod-like morphology by organic acids (citric, formic) suggests a milder hydrolytic attack. This allows for the selective removal of amorphous domains without compromising the longitudinal integrity of the crystallites. This finding is significant because it suggests that acid selection can be used as a simple, non-energy-intensive tool to tune the aspect ratio of nanocellulose, a

Table 4
Comparison of nanocellulose isolation from various sources and acid hydrolysis methods.

Source Material	Hydrolysis Agent	Particle Morphology	Crystallinity Index (%)	Ref.
Bamboo Fibers	H_2SO_4 (64 %)	Needle-like	~73 %	Brito et al. (2012)
Tea Stalk	H_2SO_4 / HCl	Rod-like	70 - 75 %	Guo et al. (2020)
Pepper Waste	Formic / H_2SO_4	Spherical & Rod	70 - 82 %	Holilah et al. (2022)
Oil Palm EFB	H_2SO_4	Rod-like	59 - 68 %	Septevani et al. (2020)
Filter Paper Waste	H_2SO_4 / HCl / Citric / Formic	Tunable: Spherical (Inorganic) & Rod-shaped (Organic)	High: 87.4 % (HCl & Citric)	**This Work**

capability that is crucial for tailoring reinforcement efficiency in polymer composites (where rods are preferred) versus drug delivery carriers (where spheres are often preferred). Table 4 summarizes how these findings compare with previous works, highlighting the superior crystallinity obtained in this study.

4. Conclusion

This study demonstrates a sustainable pathway for valorizing filter paper waste into high-value nanocellulose, addressing the critical need for circular economy solutions in laboratory waste management. The scientific novelty of this work lies in the 'acid-directed morphology control', where the simple selection of hydrolysis agent dictates the final particle shape. It was established that inorganic acids (H_2SO_4, HCl) induce a 'peeling' mechanism resulting in spherical nanoparticle networks (avg. diameter ~42–53 nm), whereas organic acids (formic, citric) act as shape-preserving agents, yielding rod-like nanocrystals. Quantitatively, the isolated nanocellulose exhibited exceptional quality. The Crystallinity Index (CrI) for HCl and Citric acid-hydrolyzed samples reached 87.4 %, which significantly exceeds benchmarks from recent studies on agricultural waste nanocellulose, such as bamboo (~73 %) and tea stalks (~75 %). Furthermore, while sulfuric acid provides colloidal stability, our EDS and TGA results confirmed that residual sulfate groups drastically reduce thermal stability (Tonset = 220 °C). In contrast, the organic acid routes produced nanocellulose with superior thermal resistance (Tonset > 280 °C) without identifying mineral residues. These findings offer a clear framework for applicability: spherical/sulfated nanocellulose is ideal for applications requiring high colloidal stability (e.g., rheology modifiers), while rod-shaped/high-crystallinity nanocellulose from organic acids is better suited for high-temperature polymer composites where thermal stability and mechanical reinforcement are paramount. Thus, this work provides a scalable, eco-friendly protocol to tailor nanocellulose properties for specific end-use requirements.

CRediT authorship contribution statement

Zahrotul Istiqomah: Writing – review & editing, Writing – original draft, Visualization, Methodology, Investigation, Formal analysis, Conceptualization. **Holilah:** Writing – review & editing, Visualization, Validation, Supervision, Investigation, Formal analysis, Conceptualization. **Didik Prasetyoko:** Writing – review & editing, Validation, Supervision, Investigation. **Sri Sunarmi:** Resources, Methodology, Investigation, Formal analysis. **Hendro Juwono:** Resources, Methodology, Investigation, Formal analysis, Data curation. **Agus Wedi Pratama:** Writing – review & editing, Visualization, Validation, Investigation, Formal analysis. **Mohd Saiful Asmal Rani:** Writing – review & editing, Validation, Supervision, Investigation, Formal analysis. **Dina Wahyu Indriani:** Resources, Investigation, Formal analysis, Data curation. **Victor Feizal Knight:** Validation, Supervision, Resources, Funding acquisition, Formal analysis. **Mohd Nor Faiz Norrrahim:** Writing – review & editing, Validation, Supervision, Investigation, Formal analysis.

Declaration of competing interest

The authors declare that they have no known competing financial interests or personal relationships that could have appeared to influence the work reported in this paper.

Acknowledgment

The authors would like to acknowledge Direktorat Riset dan Pengabdian kepada Masyarakat (DRPM) Institut Teknologi Sepuluh Nopember for the financial and technical support under Penelitian Tendik 2023 grant awarded to Zahrotul Istiqomah. We would also like to acknowledge Universiti Pertahanan Nasional Malaysia (UPNM) for the financial support received.

References

Barbosa, R.F.S., Souza, A.G., Ferreira, F.F., Rosa, D.S., 2019. Isolation and acetylation of cellulose nanostructures with a homogeneous system. Carbohydr. Polym. 218, 208–217. https://doi.org/10.1016/J.CARBPOL.2019.04.072.

Brito, B.S.L., Pereira, F.V., Putaux, J.L., Jean, B., 2012. Preparation, morphology and structure of cellulose nanocrystals from bamboo fibers. Cellulose 19, 1527–1536. https://doi.org/10.1007/s10570-012-9738-9.

Chen, S., Chen, Y., Li, D., Xu, Y., Xu, F., 2021. Flexible and sensitivity-adjustable pressure sensors based on carbonized bacterial nanocellulose/wood-derived cellulose nanofibril composite aerogels. ACS Appl. Mater. https://doi.org/10.1021/acsami.0c21392.

Chen, Y., Zhang, L., Yang, Y., Pang, B., Xu, W., Duan, G., Jiang, S., Zhang, K., 2021. Recent progress on nanocellulose aerogels: preparation, modification, composite fabrication, applications. Adv. Mater. 33. https://doi.org/10.1002/adma.202005569.

Collazo-Bigliardi, S., Ortega-Toro, R., Chiralt Boix, A., 2018. Isolation and characterisation of microcrystalline cellulose and cellulose nanocrystals from coffee husk and comparative study with rice husk. Carbohydr. Polym. 191, 205–215. https://doi.org/10.1016/J.CARBPOL.2018.03.022.

Ee, L.Y., Tan, R.P.W., Li, S.F.Y., 2022. Facile electrospray fabrication of ultralow biofouling cellulose acetate desalination membrane with nanocellulose/UiO66-NH2 fillers. J. Memb. Sci., 121200 https://doi.org/10.1016/j.memsci.2022.121200.

Emam, A.A., Abo Faraha, S.A., Kamal, F.H., Gamal, A.M., Basseem, M., 2020. Modification and characterization of nano cellulose crystalline from Eichhornia crassipes using citric acid: an adsorption study. Carbohydr. Polym. https://doi.org/10.1016/j.carbpol.2020.116202.

Firmanda, A., Mahardika, M., Fahma, F., Amelia, D., Pratama, A.W., Amalia, N., Syafri, E., Achaby, M.El, 2024. Cellulose-enriched ascorbic acid for wound dressing application: future medical textile. J. Appl. Polym. Sci. 141, e56013. https://doi.org/10.1002/APP.56013.

Guo, Y., Zhang, Y., Zheng, D., Li, M., Yue, J., 2020. Isolation and characterization of nanocellulose crystals via acid hydrolysis from agricultural waste-tea stalk. Int. J. Biol. Macromol. 163, 927–933. https://doi.org/10.1016/j.ijbiomac.2020.07.009.

Hassan, M.L., Fadel, S.M., Abouzeid, R.E., Abou Elseoud, W.S., Hassan, E.A., Berglund, L., Oksman, K., 2020. Water purification ultrafiltration membranes using nanofibers from unbleached and bleached rice straw. Sci. Rep. 10, 1–9. https://doi.org/10.1038/s41598-020-67909-3, 2020 10:1.

Holilah, Asranudin, El Messaoudi, N., Ulfa, M., Hamzah, A., Hamid, Z.A.A., Ramadhani, D.V., Suryanegara, L., Mahardika, M., Melenia, A.T., Pratama, A.W., Prasetyoko, D., 2024. Fabrication a sustainable adsorbent nanocellulose-mesoporous hectorite bead for methylene blue adsorption. Case Stud. Chem. Environ. Eng. 10, 100850. https://doi.org/10.1016/J.CSCEE.2024.100850.

Holilah, H., Bahruji, H., Ediati, R., Asranudin, A., 2022. Uniform rod and spherical nanocrystalline celluloses from hydrolysis of industrial pepper waste (Piper nigrum L.) using organic acid and inorganic acid. Int. J. Biol. Macromol. 204, 593–605. https://doi.org/10.1016/j.ijbiomac.2022.02.045.

Holilah, H., Suryanegara, L., Bahruji, H., Masruchin, N., Suprapto, S., Ediati, R., Asranudin, A., Jalil, A.A., Ramadhani, D.V., Hamid, Z.A.A., Prasetyoko, D., 2023. Nanocrystalline cellulose from lactic acid hydrolysis of pepper waste (Piper nigrum L.): response surface methodology optimization and application in bio-composite. J. Mater. Res. Technol. 27, 6344–6357. https://doi.org/10.1016/J.JMRT.2023.11.084.

Ioelovich, M., 2012. Optimal conditions for isolation of nanocrystalline cellulose particles. Nanosci. Nanotechnol. 2, 9–13. https://doi.org/10.5923/j.nn.20120202.03.

Johar, N., Ahmad, I., Dufresne, A., 2012. Extraction, preparation and characterization of cellulose fibres and nanocrystals from rice husk. Ind. Crops. Prod. 37, 93–99. https://doi.org/10.1016/j.indcrop.2011.12.016.

Khalili, E., Mehrabi, F., Korrani, Z.S., Kamyab, H., 2025. Hyssop-infused electrospun nanofiber mask for antiviral protection. Bionanoscience 15, 560. https://doi.org/10.1007/s12668-025-02186-w.

Klunklin, W., Hinmo, S., Thipchai, P., Rachtanapun, P., 2023. Effect of bleaching processes on physicochemical and functional properties of cellulose and carboxymethyl cellulose from young and mature coconut coir. Polym. (Basel) 15, 3376. https://doi.org/10.3390/POLYM15163376.

Mahardika, M., Firmanda, A., Pratama, A.W., Amelia, D., Abral, H., Fahma, F., Ilyas, R. A., Asyraf, M.R.M., 2025. Antimicrobial and antioxidant of biocomposite food packaging based on ginger tubers (Zingiber officinale). In: Sapuan, S.M., Abral, H., Jamal, Tarique, Thakur, V.K., Nazrin, A., Sherwani, S.F.K. (Eds.), Plant Tuber and Root-Based Biocomposites. Woodhead Publishing, pp. 39–59. https://doi.org/10.1016/B978-0-443-14126-3.00003-5.

Melenia, A.T., Jovita, S., Utami, D.I., Tamim, R., Holilah, H., Bahruji, H., Hamid, Z.A.A., Mubarok, F., Widiyastuti, W., Wibisono, A.T., Suprapto, S., Jalil, A.A., Prasetyoko, D., 2024. Nanocrystalline cellulose from calophyllum inophyllum shells waste by adjusting organic acid hydrolysis and optimization of reaction parameters using response surface methodology. Int. J. Biol. Macromol. 281, 135705. https://doi.org/10.1016/J.IJBIOMAC.2024.135705.

Meneguin, A., 2021. Nanocellulose/palygorskite biocomposite membranes for controlled release of metronidazole. Int. J. Biol. Macromol. 188, 689–695. https://doi.org/10.1016/j.ijbiomac.2021.08.018.

Mosleh-Shirazi, S., Abbasi, M., Kamyab, H., Kasaee, S.R., Mohamadpour, F., Vafa, E., Vaez, A., Feiz, A., Honarkar, H., Amani, A.M., Chelliapan, S., 2025. Insights into the biological efficacy of green synthesized resveratrol-templated mesoporous silica nanoparticles decorated with gold nanoparticles. J. Clust. Sci. 36, 205. https://doi.org/10.1007/s10876-025-02937-5.

Nagarajan, K.J., Balaji, A.N., Kasi Rajan, S.T., Ramanujam, N.R., 2020. Preparation of bio-eco based cellulose nanomaterials from used disposal paper cups through citric acid hydrolysis. Carbohydr. Polym. 235, 115997. https://doi.org/10.1016/j.carbpol.2020.115997.

Nitodas, S., Skehan, M., Liu, H., Shah, R., 2023. Current and potential applications of green membranes with nanocellulose. Membr. (Basel) 13, 694. https://doi.org/10.3390/MEMBRANES13080694.

Padhi, S., Singh, A., Routray, W., 2023. Nanocellulose from agro-waste: a comprehensive review of extraction methods and applications. Rev. Environ. Sci. Biotechnol. 22, 1–27. https://doi.org/10.1007/s11157-023-09643-6.

Pratama, A.W., Mahardika, M., Maulana, S., Nurfaizi, A., Hidayat, A., Holilah, H., Piluharto, B., Asranudin, A., Widiastuti, N., Mas'udi, A.F., Ilyas, R.A., Knight, V.F., Norrrahim, M.N.F., Aras, M.S.M., Haafiz, M.K.M., 2026. Valorization of agarwood (Aquilaria spp.) bark waste: Impact of a re-bleaching treatment on the physicochemical properties of extracted cellulose microfibrils. Results Chem 19, 102969. https://doi.org/10.1016/j.rechem.2025.102969.

Pratama, A.W., Mahardika, M., Widiastuti, N., Piluharto, B., Ilyas, R.A., Sapuan, S.M., Amelia, D., Firmanda, A., 2024a. Isolation and characterization of highly thermal stable microcrystalline cellulose derived from belulang grass (Eleusine indica). Case Stud. Chem. Environ. Eng. 9, 100743. https://doi.org/10.1016/J.CSCEE.2024.100743.

Pratama, A.W., Piluharto, B., Mahardika, M., Widiastuti, N., Firmanda, A., Norrrahim, M. N.F., 2024b. Comparative study of oxidized cellulose nanofibrils properties from diverse sources via TEMPO-mediated oxidation. Case Stud. Chem. Environ. Eng. 10, 100823. https://doi.org/10.1016/J.CSCEE.2024.100823.

Ramadhani, D.V., Holilah, H., Bahruji, H., Jadid, N., Oetami, T.P., Jalil, A.A., Asranudin, A., Ediati, R., Masruchin, N., Suryanegara, L., Prasetyoko, D., 2022. Effect of lignocellulosic composition of Reutealis trisperma waste on nanocrystalline cellulose properties. Biocatal. Agric. Biotechnol. 45, 102516. https://doi.org/10.1016/J.BCAB.2022.102516.

Ratna, R., Arahman, N., Munawar, A.A., Aprilia, S., 2023. Extraction, isolation, and characterization of nanocrystalline cellulose from Barangan Banana (Musa acuminata L.) peduncles waste. Indones. J. Chem. 23, 73–89. https://doi.org/10.22146/ijc.74718.

Roman, M., Winter, W.T., 2004. Effect of sulfate groups from sulfuric acid hydrolysis on the thermal degradation behavior of bacterial cellulose. Biomacromolecules 5, 1671–1677. https://doi.org/10.1021/bm034519+.

Sai Prasanna, N., Mitra, J., 2020. Isolation and characterization of cellulose nanocrystals from Cucumis sativus peels. Carbohydr. Polym. 247, 116706. https://doi.org/10.1016/J.CARBPOL.2020.116706.

Segal, L., Creely, J.J., Martin, A.E., Conrad, C.M., 1959. An empirical method for estimating the degree of crystallinity of native cellulose using the X-ray diffractometer. Text. Res. J. 29, 786–794. https://doi.org/10.1177/004051755902901003.

Septevani, A.A., Rifathin, A., Sari, A.A., Sampora, Y., Ariani, G.N., Sudiyarmanto, Sondari, D., 2020. Oil palm empty fruit bunch-based nanocellulose as a super-adsorbent for water remediation. Carbohydr. Polym. 229, 115433. https://doi.org/10.1016/j.carbpol.2019.115433.

Syafri, E., Jamaluddin, Harmailis, Umar, S., Mahardika, M., Amelia, D., Mayerni, R., Mavinkere Rangappa, S., Siengchin, S., Sobahi, T.R., Khan, A., Asiri, A.M., 2022. Isolation and characterization of new cellulosic microfibers from Pandan Duri (Pandanus Tectorius) for sustainable Environment. J. Nat. Fibers 19, 12924–12934. https://doi.org/10.1080/15440478.2022.2079582.

Velenturf, A.P.M., Purnell, P., 2021. Principles for a sustainable circular economy. Sustain. Prod. Consum. 27, 1437–1457. https://doi.org/10.1016/j.spc.2021.02.018.

Vinanthi Rajalakshmi, K.S., Balasubramanian, B., Hinnakki, H., Meyyazhagan, A., Liu, W.-C., Pappuswamy, M., Kamyab, H., Simancas-Racines, D., Paari, K.A., 2025. Fungal biopolymer-based nanoparticles for wound healing: mechanisms, applications, and future perspectives. Food Hydrocoll. Health 8, 100229. https://doi.org/10.1016/j.fhfh.2025.100229.

Wahyudi, M.S., Holilah, Bahruji, H., Prasetyoko, D., Asranudin, Pratama, A.W., Indriani, D.W., Suryanegara, L., Faradilla, R.F., Mahardika, M., Wardani, R.K., Piluharto, B., Knight, V.F., Norrrahim, M.N.F., 2025. The effect of organic acid hydrolysis on the properties of nanocellulose from edamame husk (Glycine max (L.) merill). Case Stud. Chem. Environ. Eng. 11, 101179. https://doi.org/10.1016/J.CSCEE.2025.101179.